

CosmoGen: a cosmological model generator

D. Castelão^{1,2,★} and I. Tereno^{1,2}

¹ Instituto de Astrofísica e Ciências do Espaço, Faculdade de Ciências, Universidade de Lisboa, Tapada da Ajuda, PT-1349-018 Lisboa, Portugal

² Departamento de Física, Faculdade de Ciências, Universidade de Lisboa, Edifício C8, Campo Grande, PT1749-016 Lisboa, Portugal

Received September 20, 2025

ABSTRACT

Context. The standard Λ CDM paradigm of the physical Universe suffers from well-known conceptual problems and is challenged by observational data. Alternative models exist in the literature, both phenomenological and physically motivated, many of them suffering from similar or new problems.

Aims. We propose a method to mechanically generate alternative models in a procedure informed by data and tuned to mitigate specific problems.

Methods. We implement a computational framework, dubbed CosmoGen, that integrates evolutionary algorithms for symbolic regression, with computation of structure formation and background cosmological quantities that are used to guide the evolutionary process. As a proof-of-concept we apply the procedure to the specific case of dark energy fluid models, and ask the framework to generate models capable of alleviating the cosmological tensions S_8 and H_0 .

Results. The system generates models with high fitness values, and through a Bayesian analysis of an illustrative model, we show that the model indeed alleviates the tensions.

Key words. methods: numerical – dark energy – large-scale structure of the universe – cosmological parameters

1. Introduction

A quarter of a century after its discovery (Riess et al. 1998; Perlmutter et al. 1999), the accelerated expansion of the Universe remains a central puzzle of modern cosmology. The cosmological constant, which can be included in the Einstein equations in a natural way, has been the standard way to account for the accelerated expansion, establishing the Λ CDM paradigm. While this paradigm has been successful in explaining current observations of the universe, it faces significant challenges, from the interpretation of the cosmological constant as the vacuum energy density (Weinberg 1989), through the coincidence problem (Zlatev et al. 1999), to the tensions between low and high-redshift measurements of the Hubble constant and the S_8 parameter (Planck Collaboration et al. 2014; Riess et al. 2016; Hildebrandt et al. 2017).

The theoretical investigation of dark energy alternatives to the cosmological constant as a source of the accelerated expansion is a very active field of research, and there is a long list of proposed models of various types (Di Valentino et al. 2021). Since the early days of this puzzle, a program of observational probes of dark energy was initiated (Albrecht et al. 2006). Through measurements of background-level and large-scale structure formation observables, Λ CDM was thoroughly tested and the viability of alternative models was assessed. We are currently at the start of the fourth stage of this program. Recent results of the first of the stage-IV cosmological surveys, performed with the Dark Energy Spectroscopic Instrument (DESI), favour a dynamical dark energy

(DESI Collaboration et al. 2025). The first stage-IV space-based survey, ESA's Euclid mission, started its 6-year nominal cosmological survey in 2024 (Euclid Collaboration et al. 2025), and it will be followed by the ground-based Legacy survey of Space and Time (LSST) of the Vera C. Rubin observatory (LSST Science Collaboration et al. 2009) and NASA's Nancy Grace Roman Space Telescope (Roman ROTAC and CCSDC 2025). These surveys will provide unprecedented datasets, in terms of number of tracers, image resolution, number of filters, and spectroscopic resolving power, accompanied by improvements in the handling of systematics.

The traditional way to infer dark energy properties from data is to constrain the specific parameters of physical dark energy models against data, or to constrain general features shared by various models such as the derivative of the equation of state of dark energy at a pivot point (Linder 2003). However, the vast amounts of data and improved likelihoods may also be used to guide the construction of the cosmological models themselves. This approach is nowadays possible thanks to the new computational techniques introduced by machine learning. This is the approach followed in this work, where we create phenomenological models by generating cosmological functions according to data features encoded in the likelihood. For this, we develop a framework that integrates machine learning techniques with a cosmology solver and parameter space sampling methods.

In computer science, machine learning (ML) is a field dedicated to developing methods and algorithms capable of learning from data to describe systems or perform specific tasks (Turing 1950; Carbonell et al. 1983). Based on the organization and structure of the data, ML is generally divided into two primary subfields: supervised learning and unsupervised learning

★ e-mail: dmcastelao@ciencias.ulisboa.pt

(Webb & Goode 2025). If the sample data is labeled, meaning each data point is associated with a known correct measurement, then it is a supervised learning problem. Its aim is to develop a predictive model that forecasts the future behavior of a system based on past observations. This process, also called fitting or training, involves adjusting model parameters to match the model closer with the observations. Common examples of supervised learning tasks include classification, regression, and time series modeling. If the data are unlabeled, it is an unsupervised learning problem, where the goal is to identify hidden patterns or structures within the data. Typical examples of unsupervised learning tasks include clustering and dimensionality reduction.

There are many applications of ML in physics, astronomy and cosmology (cf. Carleo et al. (2019); Fluke & Jacobs (2020), Ntampaka et al. (2019) respectively, for reviews), some of them using symbolic regression, the ML technique we use in this work. Symbolic regression (SR) (Kronberger et al. 2024a) is a type of supervised learning optimized for regression problems. Nowadays, the most used learning algorithms for SR are evolutionary algorithms inspired from principles of natural selection (Goldberg 1989; Haupt & Haupt 2004). The SR technique is capable of building functional forms by combining a set of operators, operands, and rules. Unlike classic regression techniques, which require predetermined functional forms, SR optimizes the functional form, the order of operators, and the numerical parameters. SR enables the exploration of a range of potential equations that best fit the data. A goal of SR is thus to discover “physical laws” that can be analytically expressed from the data. As an example, SR has been successfully applied in rediscovering planetary motion laws using the trajectories of the Sun, planets, and major moons in the Solar System (Lemos et al. 2023).

SR has been used in cosmology for example in studies of N-body simulations (Li et al. 2021), baryonic feedback (Wadekar et al. 2023), enhanced models of halo occupation distribution (Delgado et al. 2022), or more relevant for our goal, to generate cosmological functions (Arjona & Nesseris 2020; Koksbang 2023; Bartlett et al. 2024). Most studies that use SR to generate phenomenological cosmological functions guided by data rely only on background-level observables. In contrast, our framework *CosmoGen* uses both background and large-scale structure data, allowing the SR algorithms to explore the vast space of potential dark energy models.

CosmoGen is a new framework that integrates supervised learning symbolic regression methods with the cosmological Boltzmann code *CLASS* (Lesgourgues 2011; Blas et al. 2011) and the Bayesian inference tool *MontePython* (Audren et al. 2013). In this framework, each candidate model proposed by the SR algorithm is implemented on-the-fly as a modified version of *CLASS*, treating it as a new dark energy or dark matter component. *MontePython* then performs a preliminary parameter estimation using a likelihood tuned to the objectives we want to achieve, and returns a fitness score. The score is fed back into the evolutionary loop of the SR algorithm. This is a hybrid approach between traditional sampling methods and evolutionary strategies. The evolutionary methods are tasked with discovering functional forms, while the traditional sampling methods are responsible for evaluating each functional form and extracting the best-fit values for its parameters.

The ML part of the framework uses evolutionary methods that are introduced in Sect. 2. Section 3 describes the *CosmoGen* framework, including its prototype implementation. The framework is applied in Sect. 4 to a case study, namely the building of dark-energy fluid models generated to alleviate the Hubble and

S_8 tensions. One model from the resulting population of generated models is selected and analysed in Sect. 5, where its parameters are constrained. We conclude in Sect. 6.

2. Evolutionary methods

SR has been integrated into a wide number of evolutionary methods. These methods can be organized in the following categories (Kronberger et al. 2024a): regression-based divided in linear and non-linear methods, expression tree-based including genetic programming (Koza 1992), reinforcement learning (Sutton & Barto 2018) or transformer neural networks (Vaswani et al. 2017). There are also many variants that include several combinations of these methods, such as AI-Feynman (Udrescu & Tegmark 2020) a physics-inspired method, or symbolic metamodel (Abroshan et al. 2023) a mathematics-inspired method.

Genetic programming (GP) (Koza 1992) is a widely used evolutionary algorithm used in SR. In evolutionary algorithms, a population of solution candidates is used in a parallel search process. This approach involves repeatedly recombining, mutating, and evaluating portions of solution candidates to gradually achieve improvements. The algorithm simulates processes observed in natural evolution, particularly the inheritance of traits from parents to offspring and selection pressure. GP are tree-based expressions, composed of primitives, for example binary and unary operators such as multiplication or exponential, and terminals that represent the variables and constants used to formulate a function. These are defined in what is called a “PrimitiveSet”.

The GP algorithm proceeds as follows:

1. **Initialization:** A population of solution candidates (referred to as individuals) is randomly generated.
2. **Fitness Evaluation:** Each individual is evaluated based on a fitness function to measure its quality or how well it solves the problem.
3. **While Loop / Stopping Criteria:** Repeat the following steps until a predefined stopping criterion is met (e.g., a maximum number of generations or satisfactory fitness level):
 - (a) **Parent Selection:** A subset of individuals is chosen to be parents, typically based on their fitness values.
 - (b) **Recombination:** New individuals (children) are generated from the selected parents through recombination or crossover, creating variations in the population.
 - (c) **Fitness Evaluation of Children:** Each child is evaluated to determine their fitness.
 - (d) **Replacement:** The next population is formed by selecting individuals from the current population and the new children based on their fitness values.
4. **Return the Best Individual:** The algorithm outputs the best-performing individual from the population.

In this work, we use GP as the evolutionary algorithm because of simplicity in implementation. However, the method shows great inefficiency in the production of candidates. This is due to the fact that tree-based methods for a certain space of genotypes and for a specific tree length limit can generate multiple expressions that represent the same function (Kronberger et al. 2024b). Exhaustive symbolic regression (Bartlett et al. 2024) is an alternative method that addresses the inefficiency problems of GP in the context of cosmological model generation.

Evolutionary algorithms also need to handle a second problem, namely the problem of overfitting. For this, the algorithms

in general aim for a balance between an accurate fit and a simple equations. Indeed, while more complex functions can achieve higher accuracy on specific datasets, they tend to generalize poorly due to overfitting. Hence, limiting the model complexity is an important point, since simpler and interpretable expressions, though not always the most accurate, frequently exhibit a more reliable extrapolation behavior. Achieving this balance between accuracy and simplicity to derive the “best” equation for a given dataset requires a procedure for managing these two aspects. Several methods exist for evaluating this balance.

3. CosmoGen framework

The CosmoGen framework contains two primary components:

- The machine learning component. It consists of a symbolic regression method, which is implemented via the *Distributed Evolutionary Algorithms in Python* package (DEAP)¹. DEAP is a framework for implementing evolutionary algorithms, including but not limited to Genetic Programming.
- The cosmological component. It is linked to a modified version of CLASS.

The ML component focus on building the structure of the cosmological equation, *i.e.*, the functional form of the candidates. The choice of method used to generate a population of candidates can be adjusted with ease. Currently, the framework uses standard tree-based GP from DEAP, with minimal modifications. The cosmological component evaluates the candidates for physical viability, integrating **CLASS** computations and **MontePython** sampling methods. This second component is integrated in the GP loop, acting on points 2 and 3 of the procedure outlined in Sect. 2.

The physical interpretation of each individual depends on the desired case study and is determined by how it is integrated into the modified version of CLASS. Our framework provides a wide range of possibilities for exploration. It allows the user to consider any new cosmological component for which the relevant cosmological equations for background and perturbations can be written in a generalized form.

Fixing the generalized equations provides the Ansatz for the new cosmological component. `CosmoGen` generates new candidates considering the specific Ansatz. Three modified versions of `CLASS` can be included in `CosmoGen`, allowing for three Ansaeze: one designed for the potential of scalar fields (which can represent either scalar field dark matter or dark energy); one for a cosmological fluid (which may be dark matter, dark energy, or unified dark matter-energy); and another to explore models with couplings between dark matter and dark energy. Only the cosmological fluid case is fully implemented in the current version of `CosmoGen`.

In the case study here presented, we consider a dark energy fluid $\rho_{\text{DE}}(a)$ with no perturbations that will replace the cosmological constant in the standard Λ CDM model. This case is implemented by adding a new dark energy fluid instance to CLASS (and setting $\Omega_\Lambda = 0$).

To run CosmoGen, the following components are required:

- The DEAP Python package, which provides the evolutionary algorithms used for Symbolic Regression, along with other standard Python packages. These can be easily installed through Pip or Conda.

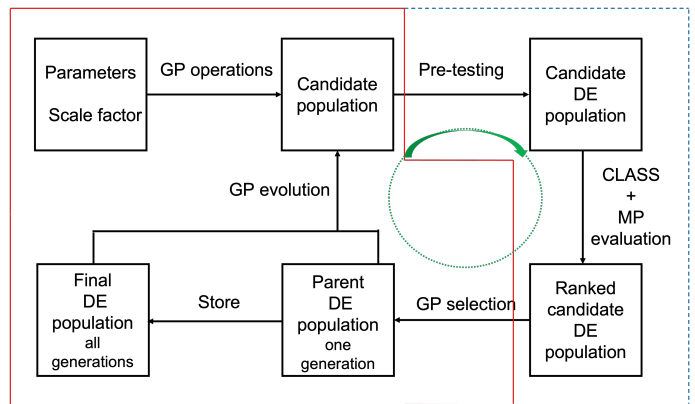


Fig. 1. Flowchart showing the sequence of steps of a CosmoGen run. The machine learning component is enclosed in the solid red border and the cosmological component in the dashed blue border. The sequence of steps moves through the two components in a loop. GP and MP stand for genetic programming and MontePython, respectively. See text for a full description.

- A compiled version of CLASS, which is used for cosmological computations.
- The MontePython code, which is employed for the optimization of the coefficients using Markov chain Monte Carlo (MCMC) methods.

`CosmoGen` contains an input file that defines the GP configuration for the simulation as well as the paths for `CLASS`, `MontePython`, and the simulation output. The code runs following the procedure described in Sects. 3.1 through 3.5, and summarized in Fig. 1.

3.1. Initial population

The algorithm begins by randomly generating an initial population of candidates by applying a predefined set of operations (*e.g.* addition, multiplication, sine, logarithm, negation) to a predefined number of variables (*e.g.* the scale factor) and coefficients (free parameters to allow different coefficients on the various terms of the functional forms generated).

3.2. Pre-testing

The evolutionary process then starts from this first generation, in an iterative loop. Each step of the loop corresponds to one generation. In each iteration, the population passes through a pre-testing procedure that filters the individuals that have the potential to be a dark energy model. The pre-testing consists of the following steps applied to each individual of the population.

- **Simplification:** The individuals are simplified using both SymPy and customized simplification methods (`smart_simplify`) that do a permutation check and a reparametrization of constants. This step ensures that the expressions are in their most reduced form for further processing.
- **Energy density:** After the simplification step, the functional forms are transformed into an energy density expression by multiplying the original functional forms by an amplitude parameter A representing an energy density parameter.

¹ <https://pypi.org/project/deap/>

- **Uniqueness check:** The framework checks if the generated individuals have been previously generated by comparing it to a history of past equations. If the expression is not unique, the individual is rejected.

- **Derivatives calculation:** The first and second order derivatives of the energy density are computed. These derivatives are needed to calculate the equation of state $w(a)$ using the continuity equation,

$$w = -\frac{a\rho'}{3\rho} - 1, \quad (1)$$

and the adiabatic speed of sound, c_s^2 , using its derivative,

$$c_s^2 = \frac{dp}{d\rho} = \frac{a\rho''}{3\rho'} - \frac{4}{3}, \quad (2)$$

where the derivatives are taken with respect to conformal time.

- **Infinities and complex number check:** The free parameters of the candidate equation are not assigned specific values at this point. To verify the validity of the expressions, it is necessary to test the free parameters across a range of values. We select three indicative values to probe their range (a value close to zero, another “mid-range” close to unity, and a large value). For each value, we evaluate $\rho(a)$, $w(a)$ and $c_s^2(a)$ to ensure that no infinities or complex values are produced. This is critical as complex values are not physically meaningful in this context. If no viable parameter values are found the model is discarded.

- **Free parameters priors:** A chi-square value is computed based on how close the equation of state $w(a)$ computed for the selected free parameters values is to a pre-defined target range. A similar computation is made for c_s^2 , where the target range is close to zero. For each model, the value of the free parameters that yield the lowest χ^2 is stored, for future indication of the parameters’ region-of-interest.

3.3. Evaluation

At this point, we have a sub-set of the population identified as possible dark energy models. The next step is the evaluation procedure, which is a core component of `CosmoGen`. The evaluation step is responsible for valuating the fitness of each individual and consists on several steps, applied in turn for each surviving individual.

- **Conversion:** The energy density expression and its derivatives are mechanically updated in the format required by the `CLASS` code using a built-in library.
- **File modification:** The background and input source files from `CLASS` are modified to include the new dark energy fluid. Input files for both `CLASS` and `MontePython` are also updated.
- **Compilation:** The modified version of `CLASS` is compiled. If the compilation is successful, `CLASS` will perform a single test run using the best free parameter value from the pre-testing phase.

- **MCMC evaluation:** `MontePython` runs an MCMC sampling the parameter space of the free parameters plus additional cosmological parameters. The free parameters are assigned priors according to the best values found in pre-testing. The choice of likelihood is a key aspect of the procedure. This is the point where the data guide the generation of the population of models. The likelihood is selected according to the problem we want to address (e.g., we may want models that alleviate cosmological tensions, or models that are optimized for a given combination of datasets, or models optimized for a certain measured feature). The MCMC is run for each model that passed the pre-testing, and for each generation, thus being a computing intensive step. For this reason the chains are kept short.

- **Fitness value:** The best χ^2 value from the MCMC is returned as the fitness value to be used in the subsequent evolutionary selection step.

3.4. Selection

At the end of the evaluation, each model has a fitness value given by the best-fit χ^2 obtained for the chosen likelihood and resulting from the short chains. We note this is not necessarily the minimum χ^2 that could be achieved with longer chains or a different parameter space.

Given the uncertainty associated with these best-fits, the next step selects a sub-set of the best-performing solutions. The selection process is implemented through a tournament method. In this approach, a set of the best individuals is randomly selected to compete. The winners of the tournaments constitute the final selection of the present generation. They are stored as part of the final population, joining the winners of all past generations.

3.5. Evolutionary strategy

At the end of each iteration, the current final population (consisting of the survivors from the current and past generations selection processes) is taken as “parents” and is used to build the next generation.

This mixed generation population is the basis to generate a new candidate population (the “children”). The process is implemented applying the so-called $(\mu+\lambda)$ evolutionary strategy. The parameters of the strategy are defined as follows:

- μ : the number of parents randomly selected from the pool,
- λ : the size of the target population,

with λ/μ being the number of offspring generated by each selected parent.

The parents are combined through the evolutionary operations *mate* and *mutate*, constrained to the chosen values of μ and λ , to build the next generation of the population.

In our implementation of the evolutionary strategy, we consider an initial population (first generation) larger than λ , the size used in subsequent generations. Starting with a larger initial population guarantees a large number of first-generation parents in the pool, preventing a fast increase of the complexity of the models through the generations.

4. `CosmoGen` run: cosmological tensions

We now turn to a proof-of-concept application of the full procedure of the `CosmoGen` framework.

Table 1. Parameters set for the evolutionary algorithm.

GP parameter	value
Operation	Add, Sub, Mul, Pow, Div, Inv, Exp, Log, Neg
Initial population size	4096
Generations	8
μ	128
λ	512
mate probability	0.5
mutate probability	0.5
max. first gen. complexity	7
max. complexity increase	2

4.1. Setup

In this application, we ask CosmoGen to generate a population of dark energy models capable of alleviating the S_8 and H_0 tensions. We restrict the population to unperturbed dark energy fluids.

4.1.1. Dark energy density

The general equation for the normalized energy density of the dark energy component is set to the following form,

$$\Omega_{\text{DE}}(a) = \frac{A}{f(a; D)}, \quad (3)$$

where A is a normalization parameter of the dark energy density, $f(a; D)$ is the function to be generated by CosmoGen, a is the scale factor, and D is a free parameter.

Replacing the cosmological constant by this new dark energy component, we can calculate the current values of the normalized dark energy density from the closure relation,

$$\Omega_{\text{DE},0} = 1 - \sum \Omega_i - \Omega_K, \quad (4)$$

with the index i represents all other standard components of the model, and K representing curvature. From $\Omega_{\text{DE},0}$ we calculate the parameter A as,

$$A = f(a = 1, D) \Omega_{\text{DE},0} \quad (5)$$

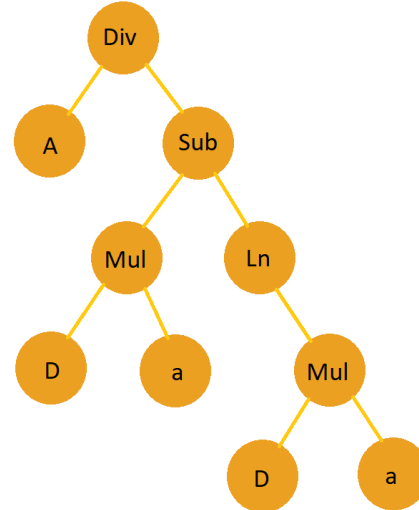
This procedure allows us to normalize the function generated by CosmoGen to expected values of the energy density. Eq. (5) can thus be rewritten as

$$\Omega_{\text{DE}}(a) = \frac{f(a = 1; D) \Omega_{\text{DE},0}}{f(a; D)}. \quad (6)$$

4.1.2. Evolutionary parameters

The population is generated by a base set of operations: (Addition, Subtraction, Multiplication, Power, Division, Inversion, Exponential, Logarithm, Negation), applied to Eq. (3). Each individual of the population is thus characterized by a certain functional form, function of the scale factor a and the free parameter D , and by the derived parameter A .

We need to set values for a number of parameters of the evolutionary algorithm. These include the size of the initial population, the number of generations (which is the ending condition for the loop), the number of parents μ , and the size of the populations of each generation (except the initial one) λ . We can

**Fig. 2.** Representation of the function $A / [Da - \ln(Da)]$ of complexity 10, as a tree generated from the GP algorithm.

also define the maximum complexity of the initial population, the maximum complexity increase from generation to generation (small values favouring simples functional forms), and the tournament size (the number of individuals that compete for a single spot). The chosen parameter values are given in Table 1.

4.1.3. Complexity

Each individual will be assigned a value of *complexity*. Representing the functional forms as trees, one can define in a natural way a measure of their complexities, as the number of nodes in the tree. The combination of two variables by an operator (multiplication, addition, subtraction, division, power) has a complexity of 3. The application of an operator to a variable or combination of variables (logarithm, exponential) has a complexity of 2. Similarly, the combination of one variable and a constant by an operator (negation, inversion, square, cube, duplication, etc.) has a complexity of 2.

Counting the nodes in the example shown in Fig. 2, for the model $A / [Da - \ln(Da)]$ that will be discussed in Sect. 5, shows this functional form has complexity 10.

4.1.4. Pre-testing

To set-up the pre-testing, we need to define the values of the free parameter D to use in the required computations of the models. We define three values (0.05, 0.95 and 1000).

We also set the target range for the equation-of-state evaluation. We chose to use a broad range of $[-15, 0]$ to allow for the possibility that the dark energy perfect fluid could be a representation of something different. Indeed, the approximation of an adiabatic perfect fluid can be applied to a specific scalar field scenario and also to various modifications of gravity (e.g., $f(R)$, torsion/non-metricity cosmologies, etc.). A broad range allows CosmoGen to explore a wider space of equations that may reveal specific behaviors of the perfect fluid consistent with certain modified gravity theories. Additionally, we also keep in mind that the resulting solutions might include parameterizations

of unknown astrophysical effects potentially occurring between early and late-time observations.

4.1.5. Integration with CLASS

We set the dark energy fluid as a replacer for the cosmological constant in the relevant locations in CLASS. For example, the Friedmann equation becomes

$$H^2(a) = H_0^2 \left[\Omega_m \left(\frac{a_0}{a} \right)^3 + \Omega_r \left(\frac{a_0}{a} \right)^4 + \Omega_{\text{DE}}(a) \right], \quad (7)$$

and we consider the dark energy fluid to be homogeneous.

4.1.6. Integration with MontePython

The evaluation step computes a fitness value for each individual. This is done by running MCMC chains with `MontePython` using the Metropolis-Hastings algorithm. The chains sample a parameter space evaluating, for each individual, the likelihoods of parameter vectors with respect to data.

As stated earlier, in this proof-of-concept, our goal is to use a dataset that will produce better fitness values for individuals that are capable of alleviating the cosmological tensions.

Cosmological tensions refer to the fact that constraints on some of the cosmological parameters are significantly different when determined using high-redshift data (namely CMB data) and lower-redshift data (namely Supernova Type Ia data probing properties of the homogeneous Universe, and weak gravitational lensing data probing the inhomogeneity of the Universe). The Hubble tension (Verde et al. 2024) is the most significant one, with more than 4σ difference between the H_0 Planck 2018 (Planck Collaboration et al. 2020) and Supernova Ia SH0ES 2022 (Riess et al. 2022) measurements. The S_8 tension shows a 2σ difference between the $S_8 = \sigma_8 \sqrt{\Omega_m/0.3}$ measurements of Planck (Planck Collaboration et al. 2020) and KiDS-1000 (Heymans et al. 2021). The subsequent KiDS-legacy analysis with better handling of weak lensing systematics has however reduced the S_8 tension to 0.73σ (Wright et al. 2025).

We therefore use the Planck 2018 CMB temperature and polarization likelihoods `Planck_high_l_TTTEEE_lite` + `Planck_low_l_EE` + `Planck_low_l_TT`, combined with a Gaussian prior for H_0 from the SH0ES 2022 estimate, and a Gaussian prior for S_8 from the KiDS-1000 estimate.

We sample a 3-dimensional parameter space consisting of the parameter D (with a flat prior around the value determined in the pre-testing for each individual), h and ω_{CDM} . The remaining cosmological and nuisance parameters are fixed to the mean values of the Planck 2018 ΛCDM estimates. For each point in the 3-d space, S_8 is derived from the other parameters. The cosmological functions used in the likelihood are the CMB power spectra computed with CLASS.

4.2. Results

One run of `CosmoGen` with this setup produces a final population of $o(10^2)$ models. For each one, we add the minimum χ^2 found in its short MCMC to its complexity, obtaining its *score*. In this way, models with more complex functional forms are penalized, although only slightly since the complexity is two orders of magnitude smaller than the χ^2 .

The 20 best models, *i.e.* the ones with the lowest scores, are shown in Table 2. We stress that the purpose of the short MCMC chains is to evaluate and select models. In other words,

Table 2. The 20 best scoring models generated by the `CosmoGen` run, showing for each model its functional form, score, minimum χ^2 and complexity.

Model	Score	χ^2_{min}	Complexity
$\frac{A}{D^3 a^3 - \ln(a)}$	637.17	627.17	10
$\frac{A}{D a^2 - a}$	638.99	629.99	9
$\frac{A}{D a^3 - a}$	640.87	629.87	11
$\frac{A}{D^2 a^2 - \ln(a)}$	642.03	632.03	10
$\frac{A}{D a - \ln(Da)}$	644.25	634.25	10
$\frac{A}{D a^3 - \ln(a)}$	645.09	635.09	10
$\frac{A}{D^3 a^{a+2} - \ln(a)}$	645.50	633.50	12
$\frac{A}{a - \ln(a^D)}$	645.65	636.65	9
$\frac{A}{D \ln(Da) - a}$	646.91	636.91	10
$\frac{A}{D^3 a - \ln(a)}$	647.15	638.16	9
$\frac{A}{a^D - \ln(a^D)}$	647.38	637.38	10
$\frac{A}{(D^2)^a}$	647.46	641.46	6
$\frac{A}{D^a \ln(Da) - a}$	647.84	635.84	12
$\frac{A}{D(a^D)^{D - \ln(a)}}$	649.14	637.14	12
$\frac{A}{D^2 a - \ln(a)}$	649.77	640.78	9
$\frac{A}{(D^3)^a}$	649.97	643.97	6
$\frac{A}{D^2 a^a - \ln(a)}$	650.19	639.19	11
$\frac{A}{D^3 a - \ln(Da)}$	650.75	639.75	11
$\frac{A}{D a^D - \ln(Da)}$	650.88	636.88	12
$\frac{A}{D(D^2 a - a^a)}$	657.09	644.09	13

a high rank shows that the model has a high likelihood for some combination of parameter values, and is a strong candidate to be selected to the final population and additionally to become a parent. This conclusion can be made even with non-converged chains, since the goal is not to estimate the posterior distribution. Therefore, this procedure does not guarantee that the model would remain among the top ranked ones after full MCMC analyses in a larger parameter space.

We select one of the top ranked models for further investigation. In Sect. 5 we investigate its features, and make a more complete MCMC analysis to verify if it indeed fulfills the goal of alleviating the tensions. For that analysis, we prefer a model with a good fitness score, low complexity, reasonably looking functional form and, if possible, resemblance with a known model. We select the fifth ranked model from Table 2.

We also make several additional runs of `CosmoGen` to compare their final populations and test the robustness of the procedure. We leave the discussion of those results to the Appendix (A).

5. Analysis of a selected model

We turn now to the analysis of the selected model, defined by the following equation for the dark energy density,

$$\rho_{\text{CG}}(a) = \frac{A}{D a - \ln(Da)}, \quad (8)$$

where the subscript *CG* stands for `CosmoGen`. This model closely resembles viable logarithmic scalar-field dark energy models discussed in the literature (see *e.g.* Wang et al. (2023)).

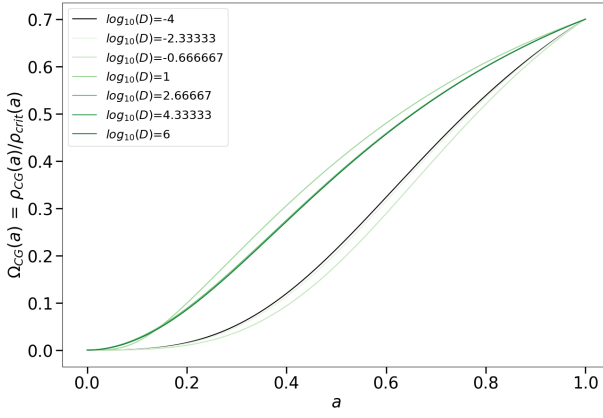


Fig. 3. Normalized energy density evolution for the CG dark energy fluid for different values of its free parameter D .

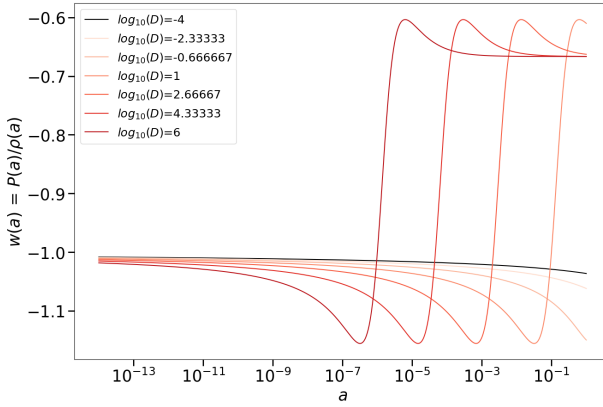


Fig. 4. Equation of state evolution for the CG dark energy fluid for different values of its free parameter D .

In Fig. 3, we show the evolution of the CG energy density, normalized to the Ω_Λ value of Planck 2018 Λ CDM model today. Defining a model through its energy density allows us to write the equation of state as function of the density and its derivatives through Eq. (1). Figure 4 shows the evolution of the equation of state of the CG fluid.

The model clearly shows two distinct behaviors. For models with positive D , the CG density increases earlier, and its equation of state crosses to the phantom regime and returns to less negative values. In contrast, models with negative D have a slow evolution of the equation of state.

Figures 5 and 6 show how the model predicted matter power spectrum and CMB temperature angular power spectrum depend on the free parameter D . Again there are two distinctive behaviors. Positive values of D can get close to Λ CDM, while negative values show deviations up to 40%, within the probed range.

We perform a likelihood analysis of the model to assess its viability and potential to alleviate cosmological tensions. For this, we no longer use the H_0 and S_8 priors that were used for model generation, but will test the model with structure formation data without imposing tension-related constraints. We make one analysis with CMB data (Planck 2018, Planck Collaboration et al. (2020)) and another with weak lensing data (KiDS-Viking KV-450, Hildebrandt et al. (2020)). We also perform an analysis of Λ CDM in the same conditions for comparison.

The parameter space consists on: the CG parameter D ; amplitude and slope of the primordial power spectrum, respectively

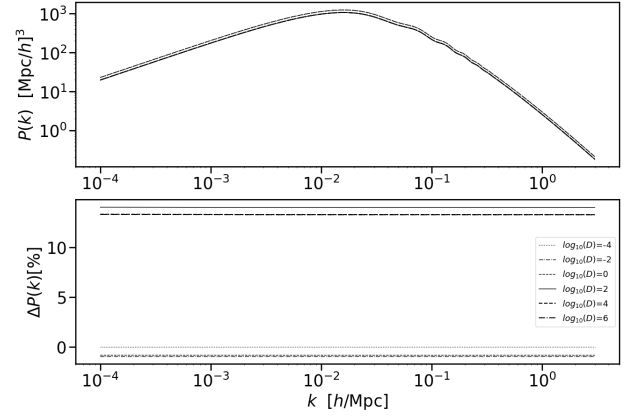


Fig. 5. *Top panel:* Matter power spectrum for the CG dark energy fluid for different values of D . *Bottom panel:* Deviation from Λ CDM.

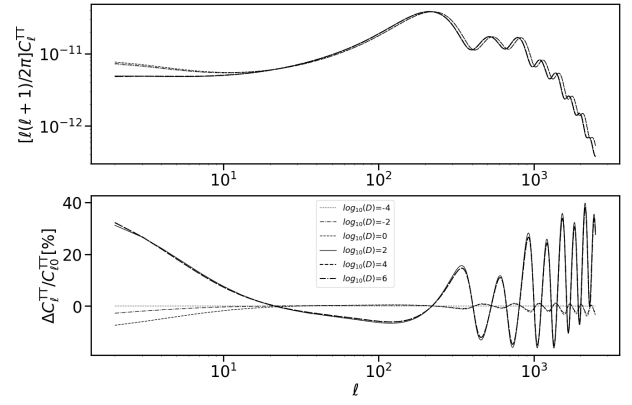


Fig. 6. *Top panel:* CMB temperature angular power spectrum for the CG dark energy fluid for different values of D . *Bottom panel:* Deviation from Λ CDM.

A_s and n_s ; baryon density (Ω_b); CDM density (Ω_{CDM}) and the Hubble constant (h). A derived parameter Ω_{DE} is calculated for the CG model, as is Ω_Λ for the Λ CDM model. The nuisance parameters used are the A_{Planck} for CMB and the amplitude of the intrinsic alignment model A_{IA} for WL. We only consider flat models, and other cosmological and nuisance parameters are kept fixed. For all parameters, the analyses are done with flat priors. For D , we consider a $\log(D)$ range of [-5, 3].

The resulting parameter constraints are shown in Table 3, and in Figs. 7 and 8. The comparison between the CG model and the Λ CDM CMB contours, in Fig. 7 (see also Table 3), shows that the CG model pushes H_0 to higher values and Ω_m to lower values. The constraints on these two parameters are broader for the CG model, but are comparable for most of the other parameters. The D free parameter is constrained to be negative, as was already hinted by the model behaviour shown in Figs. 3 to 6.

The Bayes factor, also given in Table 3, indicates a weak preference for Λ CDM. We recall that a positive value of the logarithm of the Bayes factor \mathcal{B}_{12} , between models 1 and 2, has a larger strength of evidence for model 1 (Trotta 2008).

Regarding the WL analysis, the comparison between the CG model and the Λ CDM contours, in Fig. 8 (see also Table 3), shows broad contours without significant differences between the two models.

The H_0 and S_8 tensions are better seen in Figs. 9 and 10, which compare the relevant CMB and WL contours for each of the two models. The plots show a better agreement between the

Table 3. Mean and 68% uncertainty estimates of the 6 basis parameters and 3 derived parameters for the CG and Λ CDM models from the two datasets. The Bayes factor used for model comparison is also shown.

Parameter	Planck		KiDS	
	CG Model	Λ CDM	CG Model	Λ CDM
log(D)	-2.3 ± 1.5	n.a.	$-0.8^{+3.2}_{-2.5}$	n.a.
ω_b	0.02236 ± 0.00015	0.04876 ± 0.00069	$0.0226^{+0.0028}_{-0.0020}$	$0.0401^{+0.0047}_{-0.0081}$
Ω_c	$0.249^{+0.013}_{-0.010}$	0.2582 ± 0.0076	$0.196^{+0.044}_{-0.11}$	$0.207^{+0.085}_{-0.11}$
H_0	$69.4^{+1.3}_{-1.7}$	67.88 ± 0.62	$74.2^{+7.1}_{-4.3}$	$73.8^{+6.4}_{-4.6}$
n_s	$0.9660^{+0.0045}_{-0.0050}$	0.9702 ± 0.0043	$1.03^{+0.17}_{-0.13}$	1.02 ± 0.13
$\ln 10^{10} A_s$	3.0443 ± 0.0061	3.1217 ± 0.0058	$3.46^{+1.3}_{-0.84}$	3.24 ± 0.93
Ω_m	$0.297^{+0.015}_{-0.012}$	0.3084 ± 0.0083	$0.239^{+0.046}_{-0.11}$	$0.253^{+0.066}_{-0.12}$
σ_8	$0.8246^{+0.0069}_{-0.013}$	0.8399 ± 0.0053	0.89 ± 0.16	$0.85^{+0.17}_{-0.22}$
S_8	$0.820^{+0.020}_{-0.018}$	0.852 ± 0.016	$0.757^{+0.045}_{-0.062}$	$0.737^{+0.038}_{-0.031}$
$\ln \mathcal{B}_{CG,\Lambda}$	-1.27		-0.99	

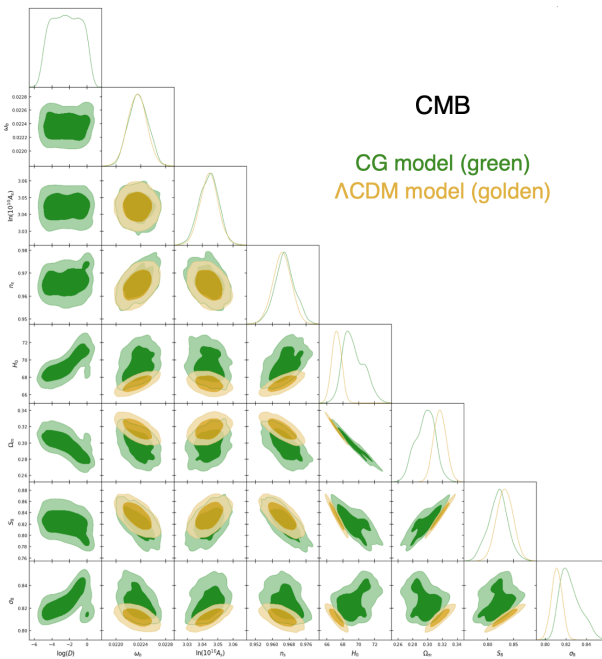


Fig. 7. CMB Planck 2018 analyses. Marginalized two-dimensional 1- and 2- σ contours of the posterior and one-dimensional marginalized posterior for the CG model (green) and Λ CDM (gold).

WL and the CMB contours in the case of the CG model. This is especially striking in contours that involve the S_8 parameter.

We compute the tension, quantifying the discrepancy between the estimates of the parameter from two different datasets, in the standard way, in terms of the combined variances of the two estimates (cf. *e.g.* Heymans et al. (2021)). We find that the CG model shows a 1.1σ S_8 tension between the datasets, while for Λ CDM we find a larger value of 2.8σ . Concerning the Hubble tension, we do not quantify it but register a 1σ shift of the Planck data H_0 CG estimate with respect to the Λ CDM one towards higher values.

We thus conclude that this case study successfully contributes to the reduction of the tensions, which is consistent with our approach of intentionally using a likelihood to that effect in the evaluation of the generated models.

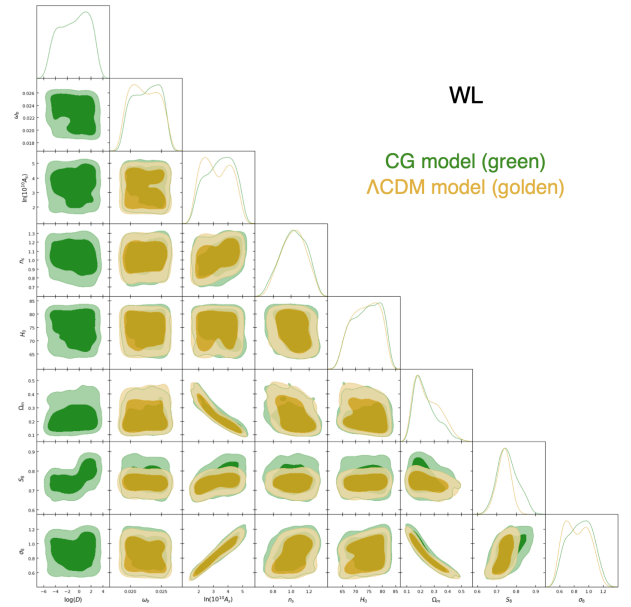


Fig. 8. WL KV-450 analyses. Marginalized two-dimensional 1- and 2- σ contours of the posterior and one-dimensional marginalized posterior for the CG model (green) and Λ CDM (gold).

6. Conclusions

We have presented a new type of cosmological tool that integrates traditional methods of numerical cosmology with ML techniques.

In the current work, we have shown an example of how this tool can provide new insights into cosmology. Incorporating evolutionary algorithms and nested sampling, the tool was applied to generate functional forms of $\rho_{\text{DE}}(a)$ that reproduce key features of observational data. Notably, CosmoGen successfully identified fluid dark energy models capable of partially resolving the S_8 and H_0 tensions.

The potential of CosmoGen is far from being fully explored. This tool has the capability to be expanded to generate other types of cosmological models, such as coupled species, unified dark matter – energy species, modified gravity theories, or also to map cosmological signatures.

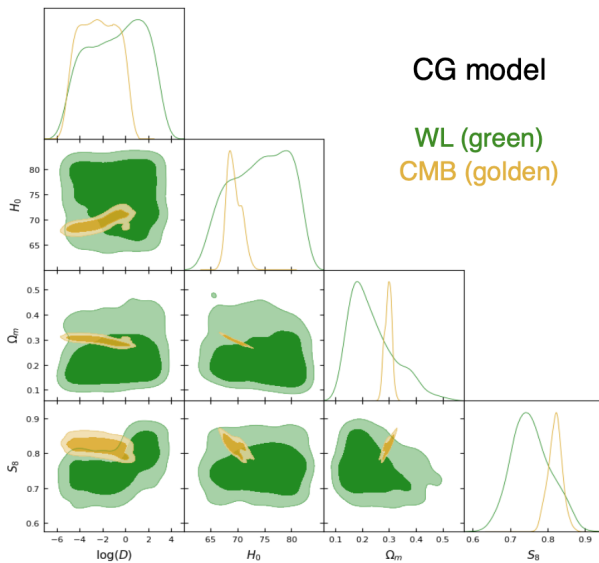


Fig. 9. CG model. Marginalized two-dimensional 1- and 2- σ contours of the posterior and one-dimensional marginalized posterior for the parameters relevant for the Hubble and S_8 tensions, for CMB Planck 2018 (gold) and WL KV-450 (green).

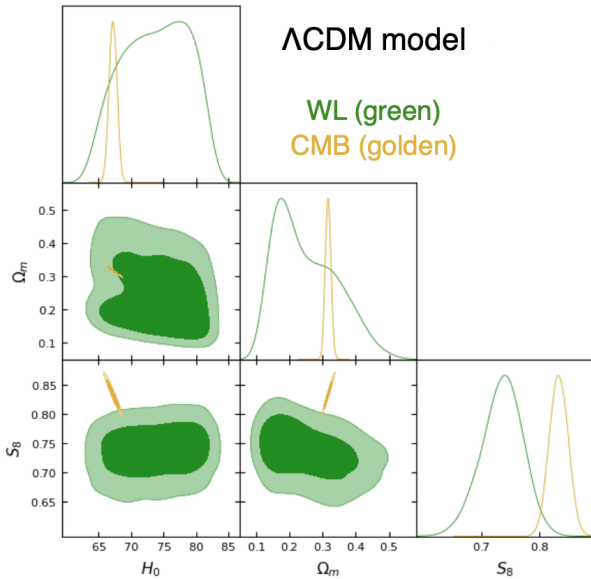


Fig. 10. Λ CDM model. Marginalized two-dimensional 1- and 2- σ contours of the posterior and one-dimensional marginalized posterior for the parameters relevant for the Hubble and S_8 tensions, for CMB Planck 2018 (gold) and WL KV-450 (green).

The results presented were obtained using a standard laptop with 16 threads. This computational limitation restricted our ability to explore the full range of mathematical functions generated in a single run, leading to lists of candidate models that were often mathematically similar. For future development, optimizing and restructuring the code is crucial. The main limitation encountered was that the stochastic GP method is not the most efficient evolutionary algorithm for sampling the space of possible equations. Further improvements of the code should incorporate alternative methods to improve the efficiency of the tool and expand its applicability. There are various other symbolic regression algorithms publicly available, most notably the

exhaustive symbolic regression, developed for cosmological applications (Bartlett et al. 2024).

Despite current limitations in sampling resolution and algorithmic efficiency, the framework demonstrates the potential of integrating AI methods with the broadly used CLASS and MontePython cosmological tools, for cosmological model building.

Acknowledgements. We thank Antonio da Silva for useful discussions and acknowledge support from the Fundação para a Ciência e a Tecnologia (FCT) through R&D Unit funding UIDB/04434/2020 and UIDP/04434/2020.

References

Abroshan, M., Mishra, S., & Khalili, M. M. 2023, in Proceedings of the AAAI Conference on Artificial Intelligence

Albrecht, A., Bernstein, G., Cahn, R., et al. 2006, arXiv e-prints, astro

Arjona, R. & Nesseris, S. 2020, Phys. Rev. D, 101, 123525

Audren, B., Lesgourgues, J., Benabed, K., & Prunet, S. 2013, J. Cosmology Astropart. Phys., 2013, 001

Bartlett, D. J., Desmond, H., & Ferreira, P. G. 2024, IEEE Transactions on Evolutionary Computation, 28, 950

Blas, D., Lesgourgues, J., & Tram, T. 2011, J. Cosmology Astropart. Phys., 2011, 034

Carbonell, J. G., Michalski, R. S., & Mitchell, T. M. 1983, in Machine Learning, ed. R. S. Michalski, J. G. Carbonell, & T. M. Mitchell (San Francisco (CA): Morgan Kaufmann), 3–23

Carleo, G., Cirac, I., Cranmer, K., et al. 2019, Reviews of Modern Physics, 91, 045002

Delgado, A. M., Wadekar, D., Hadzhiyska, B., et al. 2022, MNRAS, 515, 2733

DESI Collaboration, Abdul-Karim, M., Aguilar, J., et al. 2025, arXiv e-prints, arXiv:2503.14738

Di Valentino, E., Mena, O., Pan, S., et al. 2021, Classical and Quantum Gravity, 38, 153001

Euclid Collaboration, Mellier, Y., Abdurro'uf, et al. 2025, A&A, 697, A1

Fluke, C. J. & Jacobs, C. 2020, WIREs Data Mining and Knowledge Discovery, 10, e1349

Goldberg, D. E. 1989, Genetic Algorithms in Search, Optimization and Machine Learning (Addison-Wesley)

Haupt, R. & Haupt, S. E. 2004, Practical genetic algorithms, 2nd edn. (Wiley)

Heymans, C., Tröster, T., Asgari, M., et al. 2021, Astronomy & Astrophysics, 646, A140

Hildebrandt, H., Köhlinger, F., van den Busch, J. L., et al. 2020, A&A, 633, A69

Hildebrandt, H., Viola, M., Heymans, C., et al. 2017, MNRAS, 465, 1454

Koksbang, S. M. 2023, Phys. Rev. D, 107, 103522

Koza, J. R. 1992, Genetic Programming: On the Programming of Computers by Means of Natural Selection (Cambridge, MA: MIT Press)

Kronberger, G., Borlacu, B., Kommenda, M., Winkler, S. M., & Affenzeller, M. 2024a, Symbolic Regression, 1st edn. (Boca Raton, FL: CRC Press / Taylor & Francis)

Kronberger, G., Olivetti de Franca, F., Desmond, H., Bartlett, D. J., & Kammerer, L. 2024b, in Parallel Problem Solving from Nature – PPSN XVIII, ed. M. Affenzeller, S. M. Winkler, A. V. Kononova, H. Trautmann, T. Tušar, P. Machado, & T. Bäck (Cham: Springer Nature Switzerland), 273–289

Lemos, P., Jeffrey, N., Cranmer, M., Ho, S., & Battaglia, P. 2023, Machine Learning: Science and Technology, 4, 045002

Lesgourgues, J. 2011, arXiv e-prints, arXiv:1104.2932

Li, Y., Ni, Y., Croft, R. A. C., et al. 2021, Proceedings of the National Academy of Science, 118, e2022038118

Linder, E. V. 2003, Phys. Rev. Lett., 90, 091301

LSST Science Collaboration, Abell, P. A., Allison, J., et al. 2009, arXiv e-prints, arXiv:0912.0201

Ntampaka, M., Avestruz, C., Boada, S., et al. 2019, BAAS, 51, 14

Perlmutter, S., Aldering, G., Goldhaber, G., et al. 1999, ApJ, 517, 565

Planck Collaboration, Ade, P. A. R., Aghanim, N., et al. 2014, A&A, 571, A16

Planck Collaboration, Aghanim, N., Akrami, Y., et al. 2020, A&A, 641, A6

Riess, A. G., Filippenko, A. V., Challis, P., et al. 1998, AJ, 116, 1009

Riess, A. G., Macri, L. M., Hoffmann, S. L., et al. 2016, ApJ, 826, 56

Riess, A. G., Yuan, W., Macri, L. M., et al. 2022, ApJ, 934, L7

Roman ROTAC and CCSDC. 2025, arXiv e-prints, arXiv:2505.10574

Sutton, R. & Barto, A. 2018, Reinforcement Learning, second edition: An Introduction, Adaptive Computation and Machine Learning series (MIT Press)

Trotta, R. 2008, Contemporary Physics, 49, 71–104

Turing, A. M. 1950, Mind, LIX, 433

Udrescu, S.-M. & Tegmark, M. 2020, Science Advances, 6, eaay2631

Vaswani, A., Shazeer, N., Parmar, N., et al. 2017, in Advances in Neural Information Processing Systems (NeurIPS), 5998–6008

Verde, L., Schöneberg, N., & Gil-Marín, H. 2024, *ARA&A*, 62, 287

Wadekar, D., Thiele, L., Hill, J. C., et al. 2023, *MNRAS*, 522, 2628

Wang, D., Koussour, M., Malik, A., Myrzakulov, N., & Mustafa, G. 2023, *The European Physical Journal C*, 83 [arXiv:2304.05807]

Webb, S. A. & Goode, S. R. 2025, in IAU Symposium, Vol. 19, IAU Symposium, ed. J. McIver, A. Mahabal, & C. Fluke, 40–49

Weinberg, S. 1989, *Reviews of Modern Physics*, 61, 1

Wright, A. H., Stölzner, B., Asgari, M., et al. 2025, KiDS-Legacy: Cosmological constraints from cosmic shear with the complete Kilo-Degree Survey

Zlatev, I., Wang, L., & Steinhardt, P. J. 1999, *Phys. Rev. Lett.*, 82, 896

Appendix A: Robustness tests

We show the top ranked models from two other runs of CosmoGen in Tables A.1 and A.2.

There are some models in common between the results of the various runs. We notice, however, that models from the same run seem to share some features, while the functional forms are more distinct between different runs. For example, in the case of Table A.1 there is a strong presence of logarithms, while in Table A.2 exponentials are more prominent. This indicates that a larger initial population is required to accommodate a broad range of functions in a single run. Additionally, this highlights the lower efficiency of GP when compared to other symbolic regression methods, as discussed in Bartlett et al. (2024).

We also note that the χ^2_{\min} of these models are lower than those of Table 2. The main difference between the setups is that the evaluation MCMC chains used for Table 2 are shorter and non-converged, most likely missing the best regions of the parameters' space. It is also worth mentioning that, in contrast, the χ^2_{\min} values in Tables A.1 and A.2 are closer to the Λ CDM χ^2_{\min} for the same datasets.

It is also interesting to monitor the evolution through the generations. For this, we made new runs with longer chains, this time using the PolyChord nested sampling algorithm distributed in MontePython. An example run is shown in Table A.3. In there, we show the best models found in each of seven generations, and observe that the population globally evolves towards more complex and best-fit models.

Table A.1. The 20 best scoring models generated by a test run, showing for each model its functional form, score, minimum χ^2 and complexity.

Model	Score	χ^2_{\min}	Complexity
$\frac{A}{a^{\ln(a^2)}}$	583.17	576.17	7
$\frac{A}{(Da^2)^{\ln(a)}}$	587.12	578.12	9
$\frac{A}{-D+a-\ln(a)}$	593.76	585.76	8
$\frac{A}{(a+e^{-D\ln(a^2)})^D}$	595.20	582.20	13
$\frac{A}{(D^2a)^{\ln(a)}}$	596.48	587.48	9
$\frac{A(a^D)^D}{A}$	600.48	590.48	10
$\frac{A}{(Da)^{\ln(a)}}$	601.15	593.15	8
$\frac{A}{(2a)^{\ln(\ln(D^2))}}$	601.27	591.27	10
$\frac{A}{D^2-\ln(a)}$	603.04	596.04	7
$\frac{A}{-D^2+a-\ln(a)}$	603.51	594.51	9
$A(a^2)^a$	603.91	597.91	6
$A(e^{Da^a})^a$	604.06	594.06	10
$\frac{A}{D-\ln(a)}$	604.87	598.87	6
$Ae^{a(Da)^a}$	604.94	594.94	10
$A(e^{a^{a+1}})^D$	605.96	596.96	9
$A(e^{D\ln(a^2)})^a$	606.44	596.44	10
Aa^D	606.59	601.59	5
$\frac{A}{-D^2a^{D+1}+a-\ln(a)}$	608.02	594.02	14
Ae^a	609.35	605.35	4

Table A.2. The 20 best scoring models generated by a comparison run, showing for each model its functional form, score, minimum χ^2 and complexity.

Model	Score	χ^2_{\min}	Complexity
Aa	587.96	584.96	3
Aa^D	591.81	587.81	5
$Ae^{D\ln(a)}$	591.90	584.90	7
$\frac{A}{-D+a-\ln(a)}$	592.30	583.30	8
$A(Da)^{2D}e^{-a}$	593.86	582.86	11
$Ae^{D\ln(2a)}$	594.28	586.28	8
$\frac{A}{a^{-D-a+1}}$	595.95	586.95	9
$Ae^{a-a^{\ln(a^a)}}$	596.85	585.85	11
$-\frac{A}{D(a^a)^{\ln(a)-D^{a+1}}}$	597.19	581.19	16
$A(2a)^{(a^a)^a}$	597.20	587.20	10
$\frac{A}{(e^{2a\ln(a)})^D}$	597.86	587.86	10
$\frac{Aa^{a^a}}{a^{a^a+1}+1}$	598.27	581.27	17
$A(2a)^{(a^a)^D}$	598.76	588.76	10
$\frac{A}{D-\ln(D+a)}$	599.09	591.09	8
$Ae^{a+a^D-a^a}$	599.20	587.20	12
$Aa^{a-a\ln(a)}$	599.95	589.95	10
$Ae^{a+a^D-(a^D)^a}$	600.46	586.46	14
$A(2a)^{a^D}$	601.43	593.43	8
Ae^a	602.72	598.72	4
$\frac{A}{D-a(D+a)-a+e^a}$	606.55	592.55	14

Table A.3. The 5 best models of each generation in the Polychords run, showing functional forms, scores, minimum χ^2 , complexities and the mean complexity of each generation.

Generation	Model	Score	χ^2_{min}	Complexity	<Complexity>
1	$\frac{A}{D^{\ln(a)}}$	1000.33	994.33	6	6.0
	$\frac{A}{\ln(Da)}$	1016.10	1010.10	6	
	$\frac{A}{D^a}$	1022.98	1017.98	5	
	$\frac{A}{D-\exp(a)}$	1043.76	1037.76	6	
	$-\frac{A}{D-\exp(a)}$	1045.49	1038.49	7	
2	$\frac{A}{(D+a)^{\ln(a)}}$	950.95	942.95	8	6.2
	$\frac{A}{D^{\ln(2a)}}$	1003.96	996.96	7	
	$A D^{-a-1}$	1021.55	1016.55	5	
	$A D^a$	1021.84	1016.84	5	
	$-\frac{A}{D^a}$	1023.00	1017.00	6	
3	$\frac{A}{(D^a+a)^{\ln(a)}}$	953.16	943.16	10	9.0
	$\frac{A}{(a^2 \exp(a))^{\ln(a)}}$	965.72	955.72	10	
	$\frac{A}{D^a(D^a+a^2)}$	989.72	979.72	10	
	$\frac{A}{(2D)^{\ln(a)}}$	1000.83	993.83	7	
	$\frac{A}{(D(a+1))^a}$	1010.40	1002.40	8	
4	$\frac{A}{(Da^3)^{\ln(a)}}$	890.24	881.24	9	10.0
	$\frac{A}{(D(D-a)+a)^{\ln(a)}}$	955.01	943.01	12	
	$\frac{A \cdot a^{-\ln(a)-1}}{D^a}$	970.26	959.26	11	
	$\frac{A}{a^2 - \ln(a^2)}$	973.91	965.91	8	
	$A D^{-D^a - \ln(a)}$	978.60	988.60	10	
5	$\frac{A}{(2D a^3)^{\ln(a)}}$	887.53	877.53	10	11.0
	$\frac{A}{(D^2 a^3)^{\ln(a)}}$	889.29	879.29	12	
	$\frac{A}{(a^3 \exp(a^D))^{\ln(a)}}$	891.02	879.02	10	
	$A (2a)^{D-\exp(a)}$	911.57	903.57	14	
	$\frac{A}{(D^{a^2} + a^2)^{\ln(a)}}$	916.64	902.64	9	
6	$\frac{A}{(Da^6)^{\ln(a)}}$	846.89	837.89	9	10.4
	$\frac{A}{(Da^3)^{\ln(a^2)}}$	848.70	838.70	10	
	$\frac{A}{(D^2 a^3)^{\ln(a^2)}}$	850.92	839.92	11	
	$\frac{A}{(Da^5)^{\ln(a)}}$	856.78	847.78	13	
	$\frac{A}{(Da^3)^{\exp(a) \ln(a)}}$	859.92	846.92	9	
7	$\frac{A}{(D^2 a^3)^{\ln(a^3)}}$	832.30	821.30	11	13.2
	$\frac{A}{(a^3 \exp(a^D))^{\ln(D^a+1-a^2)}}$	842.40	824.40	18	
	$\frac{A}{(2Da^6)^{\ln(a)}}$	846.38	836.38	15	
	$\frac{A}{(Da^4 \exp(a)^{\exp(a)})^{\ln(a)}}$	851.07	836.07	10	
	$\frac{A}{(D^2 a^3)^{\ln(2a^2)}}$	852.34	840.34	12	